Document downloaded from:

http://hdl.handle.net/10251/184037

This paper must be cited as:

Galindo, J.; Climent, H.; Navarro, R.; Miguel-García, J.; Chalet, D.; Pretot, P. (2021). A study on the high pressure EGR transport and application to the dispersion among cylinders in automotive engines. International Journal of Engine Research. 22(10):3164-3178. https://doi.org/10.1177/1468087420969263

The final publication is available at

https://doi.org/10.1177/1468087420969263

Copyright SAGE Publications

Additional Information

This is the author's version of a work that was accepted for publication in International Journal of Engine Research. Changes resulting from the publishing process, such as peer review, editing, corrections, structural formatting,
and other quality control mechanisms may not be reflected in this document. Changes may have been made to this work since it was submitted for publication. A definitive version was subsequently published as https://doi.org/10.1177/1468087420969263

A study on the high pressure EGR transport and application to the dispersion among cylinders in automotive engines

José Galindo [a], Héctor Climent [a], Roberto Navarro [a], Julián Miguel-García [a], David Chalet [b], Pierre-Emmanuel Pretot [b]

[a] CMT Motores Térmicos, Universitat Politècnica de València, Spain
[b] LHEEA, École Centrale Nantes, France

Abstract

The objective of this study is to explore the limits of a one-dimensional model to predict the movement and mixing of the air and exhaust gases recirculation (EGR) flows in compact intake manifolds of recent automotive engines. In particular, the high pressure EGR loop configuration is evaluated in this study from the perspective of the EGR dispersion among cylinders.

The experimental work includes the use of a fast CO_2 tracking system that provides crank-angle resolved results in six locations of the intake manifold together with the acquisition of the time-averaged CO_2 concentration in all the intake pipes (eight locations) to evaluate the EGR dispersion empirically. A specific system was developed to inject the EGR in three locations of the intake manifold in a flexible way to modify the dispersion. Up to 29 engine running conditions defined by engine speed, engine torque and EGR rate, spanning the entire engine map, including full load operation, were evaluated.

A one-dimensional engine model was built to detect the limits in reproducing the EGR transport in the intake manifold and quantify the accuracy when predicting the dispersion among cylinders. The study concludes that the predicted EGR rate in the cylinders may differ up to 75% from the experimental measurement at low engine averaged EGR rate. The model prediction improves to differences lower than 40% in EGR rate per cylinder if the engine operating points with an EGR rate lower than 10% are excluded. In this situation, 80% of the predicted in-cylinder EGR rates have differences lower than 25% when compared to experiments.

Acronyms

AE	Absolute error
BMEP	Brake mean effective pressure
CF	Convexity factor
CFD	Computational Fluid Dynamics
COV	Coefficient of variance
EGR	Exhaust gases recirculation
HP	High pressure
LP	Low pressure
MRE	Maximum relative error
ndRMSE	non-dimensional root mean squared error
RE	Relative error

SF	Symmetry factor
VGT	Variable geometry turbine

1. Introduction

Nowadays the automotive industry is facing a challenging situation. The climate change and the health of the people are considered remarkable issues for the population. In recent years, the fuel consumption or the CO_2 emissions are in the focus of the research in the field of the use of internal combustion engines as the main powertrain system in automotive applications. In addition, NOx and smoke emissions are also considered relevant topics in Diesel units. Because of that the research efforts and the incoming laws are increasing and developing in this way.

A widely use strategy to reduce the NOx emissions in Diesel engines and improve fuel economy in gasoline ones is known as exhaust gas recirculation (EGR) [1, 2]. The performance and the effectiveness of the EGR is based on the reduction in the peak combustion temperature and the oxygen concentration as explained by Ladommatos et al. in 1996 and 1997 [3-6].

In the recent past, the range of the application of the EGR was restricted to New European Driving Cycle (NEDC) and Euro normatives. It was low speed and low load. Nevertheless the new normatives and homologation cycles are considering more realistic working operations like real driving emissions test (RDE) [7] and lower temperatures [8], both of them studied by Luján et al. in 2017 and 2018 respectively, and more frequent engine transient operations [9] studied by Galindo et al. in 2017.

These new requirements are accompanied by new challenges to overcome like the effect of the condensation when EGR mixes with ambient low temperature air. This effect was studied to predict the condensation rate by Serrano et al. in 2018 [10] and by Galindo et al. who studied the effect of the condensation in the rotor of the compressor in 2019 [11]. New EGR strategies are developed to comply the new requirements related to new transient operation marked by RDE or the Worldwide Harmonized Light vehicles Test Procedures cycles (WLTP) [12] studied by Luján in 2018.

There are two main engine configurations to perform the EGR strategy: high pressure (HP) and low pressure (LP). They are different strategies, with their own advantages and disadvantages depending on the context. In fact, nowadays there are a lot of vehicles that have both of them, which enables a better adaptation to more complex strategies required to achieve the anti-pollutant standards, increasingly demanding.

This study is focused on the HP EGR, particularly on the prediction capability of a one-dimensional model to reproduce the EGR transport inside the intake manifold and, finally, the dispersion among the cylinders, which is one of the characteristic disadvantages of the HP EGR. The dispersion of the EGR among cylinders has a negative effect over NOx and smoke emissions in diesel engines [13] and is of increasing interest in gasoline engines since an uneven repartition of the exhaust gases may lead to undesirable combustion issues. Due to these negative consequences is important trying to reduce the level of the dispersion effectiveness.

Computational codes, numerical simulations and modeling tools are widely used in engines research to predict fluid dynamics behavior. From 0D to 3D including 1D there is a lot of literature background. This kind of study is very useful because it is resource-efficient, it does not need a complex computing infrastructure and it also provides information about flow variables which are not possible to measure experimentally. These tools have been improved over the years and they are widely used by the industry when developing new engines. Although reliable and accurate to some extents, these techniques have limits. This study explores those limits too.

The application of modeling tools to engine research is diverse. Baratta et al. studied deeply the 0D combustion models and 1D simulation applied to internal combustion engines in 2011 [14]. In 2019 Korsunovs et al. evaluated a zero-dimensional stochastic reactor modeling to predict NOx emissions [15]. Poubeau et al. [16] developed a methodology and used the 1D and 3D modeling to study the benefits of thermal insulation in the combustion chamber, which was an issue previously studied, by modeling and experimentally, by Andruskiewicz et al. in 2017 [17, 18]. In 2019 Galindo et al. examined numerous extrapolation methods to study off-design conditions of the compressor map for 0D and 1D engine simulations [19]. In 2006 Bobhbot et al. performed a methodology based on a direct temporal coupling between 1D simulation software and 3D combustion code to improve the engine performance and the prediction of the emissions [20]. Different dimensional modeling have advantages and disadvantages. Ones depends of each other to work correctly. From this point of view, as long as the limits are more explored and expanded, more realistic will be the results obtained.

Concerning the modeling application on EGR, in 2012 Millo et al. presented a study where 1D model was built to evaluate the opportunities of a dual loop EGR system (combining a short route and a long route) [21]. More specifically, regarding the EGR dispersion, in 2001 Siewert et al. performed an investigation combining CFD and experimental tools [22] where two manifolds were developed to reduce the EGR dispersion and CFD analysis to understand the causes of the high dispersion. Later, in 2013, a study about the effect of the EGR dispersion on NOx and smoke tradeoff was performed by Lakhlani et al. In that study a combined modeling between 1D and CFD was useful to understand better the behavior of the EGR dispersion [23]. Finally, in 2015, a research realized by Dimitriou et al. [24] combined experimental and modeling tools and provided a thorough analysis of the geometry in the EGR dispersion, since they analyzed ten different configurations combining 1D and 3D modeling.

Most of the studies found in the literature combine 1D and 3D modeling; the former to provide boundary conditions to the latter, which is devoted to calculate the fluid-dynamics inside the intake manifold. The novelty of this study lies in three assets: (i) it quantifies the accuracy of a full 1D engine model when calculating the EGR dispersion since several dispersion levels were analyzed in each engine operating point, (ii) it compares 1D results concerning gases concentration with experimental ones in the crank-angle degree domain, and (iii) the work is developed in a state-of-the-art automotive engine with the EGR strategy activated in a wide engine running conditions, including full load operation, where there is a lack of data in the literature.

The paper is structured as follows. The experimental setup and the modeling tools are described in Section 2 and Section 3 respectively. Section 4 presents the model assessment in terms of crank-angle resolved results by comparing with the experiments. Section 5 contains the main results and the discussion in terms of the EGR dispersion prediction capability of the 1D model. Finally, main conclusions are presented in Section 6.

2. Experimental setup

The experiments are performed on a test bench with a turbocharged diesel engine. Table 1 shows the main features of the engine. The engine includes both LP and HP EGR systems, although this study is focused only in the HP EGR loop, whose schematic layout is depicted in Fig. 1. The original engine configuration concerning the intake manifold was modified with the following features: (i) an additional hardware consisting in 8 straight pipes was placed between the intake manifold and the engine block, where average CO_2 probes are placed to measure gas concentration in each intake pipe, and (ii) the EGR introduction in the intake manifold is performed by using three branches (one on the center and two on lateral locations in the manifold) together with three corresponding valves that can be manually adjusted to promote different EGR dispersion levels during the tests.

Table 1

Engine specifications.

Cylinder number	In-line 4
Bore x stroke (mm)	80x79.5
Displacement (cm^3)	1600
Compression ratio	15.4:1
Valve number	4/cylinder
Fuel delivery system	Common rail. Direct injection.
EGR system	HP and LP cooled EGR
Intake boosting	Turbocharger with VGT
Intake cooling system	Air charge air cooler (ACAC)
Maximum power (kW/rpm)	96/4000
Maximum torque (Nm/rpm)	320/1750

To determine the dispersion of the EGR rate in each intake pipe, the CO_2 concentration is measured and up to eight probes were installed in the adapted hardware in the intake. The probes were connected to a Horiba MEXA 7170DEGR, which is a conventional gas analysis system widely used in engine testing in steady conditions. Each probe had a valve that controls the gases flow to the gas analyzer. The corresponding valve was opened meanwhile the others were closed to measure only the gas composition from one pipe.

As stated before, a home-made device was installed between the HP EGR line and the intake manifold with three pipes and three regulation valves (one per branch) to control the HP EGR dispersion. The EGR branches discharged in the intake manifold in three locations: one pipe was located on the left, other was located on the right and the third

one on the center, at the top of the manifold, as in the original manifold configuration. Each pipe contained a regulation valve to control the HP EGR dispersion with high accuracy as observed in Fig. 1.

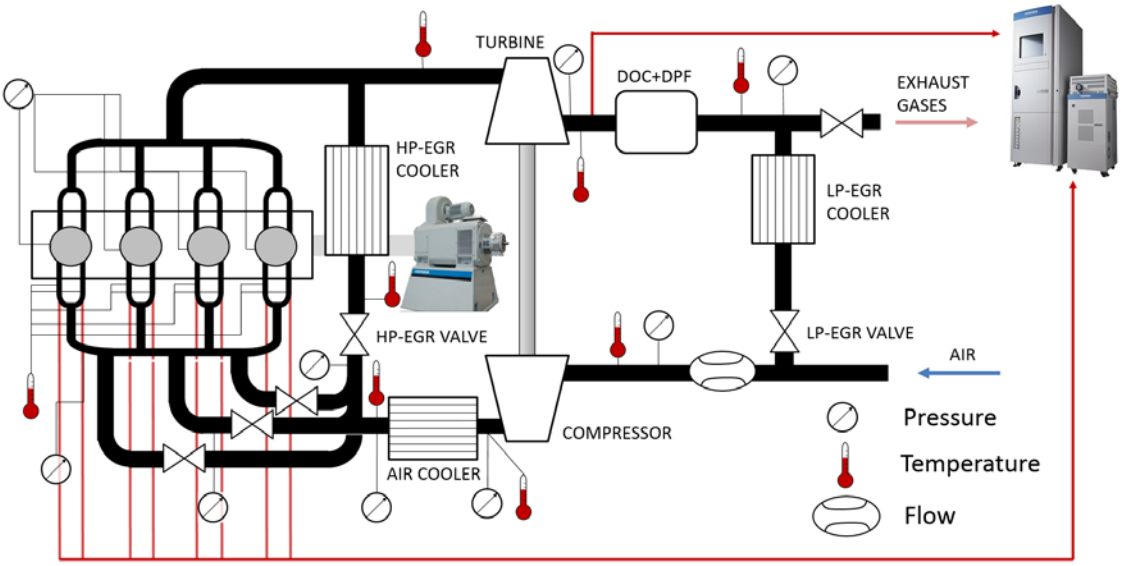

Figure 1. Engine schematic layout and CO_2 measurement detail in the cylinders.

Different sensors, which are also depicted in Fig. 1, were installed additionally to measure different engine parameters, which help to set the steady engine conditions to perform the tests. Some of them collect time-averaged values, such as pressure and temperature in relevant engine locations, while others acquire crank-angle resolved pressure traces in the cylinder, in the intake manifold and in the EGR line. They also offer relevant information to calibrate properly the 1D engine model. The variables together with the sensors features are presented in Table 2.

Table 2

Instrumentation accuracy

Sensor	Variable	Accuracy at Full Scale [%]	Range
Thermocouples type K	Temperature	1	0 ºC – 1260 ºC
Pressure sensor	Pressure	0.3	0 - 6 bar
Pressure sensor	Pressure	0.05	0-150 bar
Gravimetric fuel balance	Fuel mass flow	0.2	0 - 150 kg/h
Hot wire meter	Air mass flow	1	0 - 720 kg/h
Dynamometer brake	Torque	0.1	0 - 480 Nm
Smoke Meter	Soot	0.5	0 – 32000 mg/m3

A CO_2 fast tracking system, based on Non-Dispersive Infra-Red measuring principle, was used to evaluate the transport of exhaust gases in the intake line. The CO_2 tracking system is able to detect changes in gas concentration with a T_{90} of 8 ms, which is a higher sampling frequency than other conventional gas analysis systems, like the HORIBA MEXA 7170DEGR. The fast tracking system is able to measure with two probes at the same time. Since up to six locations in the intake manifold are used for the 1D model assessment, engine tests have to be repeated three times in a row to provide the needed data. Special care was paid to ensure the repeatability of the engine running point stabilization so the diesel particulate filter was removed in these tests and replaced by a device that provided a similar pressure drop in a specific particulate matter load conditions.

The six locations for the instantaneous measurement of the CO_2 concentration are depicted in Fig. 2. Location #1 and #2 are placed in the intake manifold; #1 is in front of cylinder 1, that is, facing a cylinder in one of the extremes of the engine block, while #2 is in a location between location #1 and the EGR discharging central branch. Locations #3, #4, #5 and #6 are placed directly in the intake pipes of cylinders 3 and 4.

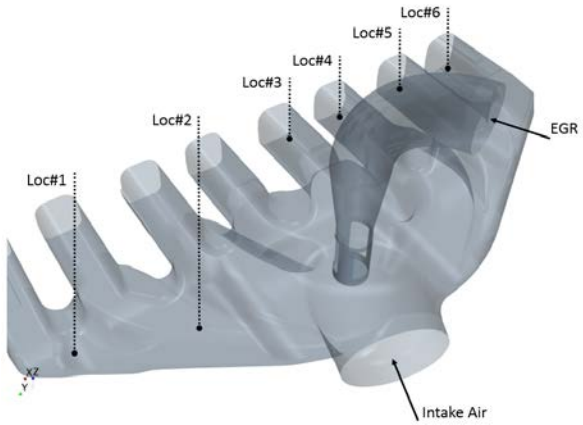

Figure 2. Intake manifold representation with the six locations for the fast CO_2 tracking system.

Engine tests in steady conditions were performed to analyze the dispersion of the HP EGR. First, it was necessary to determine the operating points taking care to study a large range over the engine map in both engine speed and brake mean effective pressure (BMEP). The EGR rate was determined under two restrictions: the first one was to study a large range between low and medium EGR rate, and the second one was to keep margin to be able to modify the HP EGR dispersion taking into account the effect on the engine stability, highly affected when the air to fuel ratio approaches to stoichiometric conditions. As stated in the Introduction section, following the current trend to perform EGR at full load operation, which was avoided several years ago, three engine running conditions are chosen in the full load curve. The final engine running conditions are presented in Table 3. In some of these engine running conditions several EGR rates were tested.

Table 3

Working operation points

N [rpm]	BMEP [bar]	Intake P [mbar]	EGR rate [%]	Engine Torque [Nm]
1250	11	1500	6	140
1500	1	1000	7, 22, 29,42	13
1500	3	1040	3, 10, 20	38
1500	15	1900	5	191
2000	6	1250	5, 15, 22, 30	76
2500	10	2100	3, 7, 17	129
2500	11.7	2300	20	149
2500	19	2660	4	231
3000	20	2750	12	254

In each operating point the values shown in Table 3 had to be kept constant so the control strategy during the tests was based on two engine controls at steady conditions. The first one was the engine torque, which was controlled by the injected fuel. And the second one was the intake manifold pressure, which was controlled by the Variable Geometry Turbine (VGT) position by means of a look-up table in the ECU calibration.

The process to perform the tests was always the same for every operation point. The configuration of the three valves to control the HP EGR dispersion was set before starting the engine. After that, the engine was started and the operation point was set (speed, torque and intake manifold pressure). It was necessary to wait to stabilize the temperature of the engine to fulfill real steady conditions. The testing procedure started with the acquisition of CO_2 concentration in the intake pipes and intake air sequentially. It required a few seconds to stabilize the measurement and obtain an accurate result, between ten and twenty seconds per pipe, depending on the working operation point.

Horiba MEXA 7170DEGR is the equipment that measures the time-averaged pollutant emissions. It acquires the CO, CO_2, THC, O_2 and NOx concentrations. It is not possible measure the EGR rate directly, so it is necessary a conversion from the exhaust and intake CO_2 concentration measurements [25] following the next expression:

$$EGR = \frac{[CO_2]_{Intake} - [CO_2]_{Ambient}}{[CO_2]_{Exhaust} - [CO_2]_{Ambient}} \quad (1)$$

Where *intake* indicates the intake pipe under measurement, *ambient* means the atmospheric concentration and *exhaust* represents the measurement in the exhaust line upstream the turbine, where the HP-EGR line is placed.

3. Modeling tools

It is possible to simulate the flow behavior inside internal combustion engines with the aid of computer codes. Historically, modeling tools are widely used in engines research. Intake and exhaust lines in engines are composed of long pipes in which the flow can be considered one-dimensional (when the length-to-diameter is high enough and the turbulent flow is totally developed). So, the most important axis is in the direction of the movement of the flow, X axis. Essentially, Z axis and Y axis are not relevant. This is important because the calculation time is significantly reduced. It is possible to propose a hyperbolic system of partial differential equations thanks to the simplification of one-dimensional Euler equations for unsteady compressible non-homentropic flow [26]. The symbolic vector form is represented in Eq. (2):

$$\frac{\partial \mathrm{W}}{\partial \mathrm{t}} + \frac{\partial \mathrm{F}}{\partial \mathrm{x}} + C1 + C2 = 0 \tag{2}$$

Where W corresponds to the mass, momentum and energy aggrupation terms, F is the flux of these terms and C represents the source terms. In Eq. (2), the more basics source terms are included, which take into account the friction, the area changes and the heat transfer effects. Nevertheless, it would have source additional terms, which are not defined in Eq (2), but they take into account other less influential effects like viscosity. The strong conservative form of Eq. (2) is represented in Eq. (3) [27]:

$$\begin{aligned}
W\,(x,t) &= \begin{bmatrix} \rho \mathrm{F} \\ \rho \mathrm{uF} \\ F\,\left(\rho\frac{u^2}{2} + \frac{p}{\gamma-1}\right) \end{bmatrix} \\
F\,(W) &= \begin{bmatrix} \rho \mathrm{uF} \\ \left(\rho u^2 + \mathrm{p}\right) \mathrm{F} \\ uF\,\left(\rho\frac{u^2}{2} + \frac{\gamma p}{\gamma-1}\right) \end{bmatrix} \\
C1(x,W) &= \begin{bmatrix} 0 \\ -p\,\frac{dF}{dx} \\ 0 \end{bmatrix} \\
C2(W) &= \begin{bmatrix} 0 \\ g\rho F \\ -q\rho F \end{bmatrix}
\end{aligned} \tag{3}$$

Furthermore, an estimation of the inclusion of the chemical species transport equation to the governing equations system is possible with the same accuracy than applied numerical methods and without changes on the resolution techniques. A total of n-1 equations considering chemical species conservation in the governing equations system is required, where n is the number of the chemical species to be transported, to solve the transport of the chemical species along the 1D elements. The vector form of the chemical species conservation equation is represented in Eq. (4):

$$\frac{\partial(\rho Y F)}{\partial t} + \frac{\partial(\rho u Y F)}{\partial x} = \rho F \dot{\mathrm{Y}}, \tag{4}$$

Where Y expressed is a vector that includes the mass fraction of n−1 different chemical species. The Eq. (5) is a compatibility equation that gives the mass fraction of the chemical species n:

$$Y_n = 1 - \sum_{j=1}^{n-1} Y_j, \tag{5}$$

The inclusion of the chemical species in the governing equations is represented in Eq. (6):

$$W(x,t) = \begin{bmatrix} \rho F \\ \rho u F \\ F\left(\rho\frac{u^2}{2} + \frac{p}{\gamma-1}\right) \\ \rho F Y \end{bmatrix}$$
$$F(W) = \begin{bmatrix} \rho u F \\ \left(\rho u^2 + p\right) F \\ uF\left(\rho\frac{u^2}{2} + \frac{\gamma p}{\gamma-1}\right) \\ \rho u F Y \end{bmatrix} \tag{6}$$
$$C1(x,W) = \begin{bmatrix} 0 \\ -p\frac{dF}{dx} \\ 0 \\ 0 \end{bmatrix}$$
$$C2(W) = \begin{bmatrix} 0 \\ g\rho F \\ -q\rho F \\ \rho F \dot{Y} \end{bmatrix}$$

As commented before, the resolution of these equations requires the use of numerical methods. Depending on the problem to solve, the numerical method employed by the software could variate according to the adaptation of the different methods to the needed resolution.

In engine geometries where there is not a prominent flow direction, a 0D approach can be employed too. These elements are widely employed because they consume less computational resources and, therefore, they are faster solving the flow governing equations. Moreover, a very relevant characteristic of 0D elements to this study is that they are able to accumulate mass inside them. So, the flow conditions are spatially homogeneous wherever inside them. In the model, some elements work in this way. The filling and emptying model is used to solve the equation system in 0D elements. The mass and energy conservation equation for an open system are applied as well as the ideal gas state equation. However, the momentum conservation equations are not applied in 0D elements.

The inclusion of the chemical species in the equation system requires the addition of n-1 equations, just like before.

$$\Delta m_{in_{Y_j}} = \sum_i \dot{m}_i Y_{jCC_i} \Delta t \tag{7}$$

Where $m_{in_{Y_j}}$ expressed in Eq. (7) represents the mass of the chemical species j inside the 0D element and Y_{jCC_i} represents the mass fraction of the chemical species j entering to or exiting from the 0D element through the boundary condition i. Finally, the mass fraction of the chemical species j at time instant is expressed in Eq. (8):

$$Y_j = \frac{m_{in_{Y_j}} + \Delta m_{in_{Y_j}}}{m_{in} + \Delta m_{in}} \quad (8)$$

Like before, the Eq. (5) is a compatibility equation that gives the mass fraction of the n chemical species [28]. The species considered in the model of the present study are air, burned gas and fuel.

The intake manifold in the present study is approximated by a combination of pipes (1D elements) and volumes (0D elements), which are connected with junctions in a convenient manner. For these junctions, the following characteristics are defined: volume, expansion diameters, characteristic length, and boundary angles. If the geometry is quite complex, the friction multipliers, heat transfer multipliers, and pressure losses coefficients are adjusted. The maximum diameter that the flow may expand to after entering a boundary is named the expansion diameter. It is used in order to model the contraction and expansion losses.

A specific software to import the geometry of the intake manifold from a computer-aided design (CAD) file to the 1D modeling was used. Then it is important to describe the manifold with a set of volumes and ducts connected with junctions. The orientation of the angles of the ducts is crucial to obtain reasonable results according to EGR dispersion.

The combustion profile of the cylinder is essential to obtain a predictive model in terms of engine performance and hot gases residuals. Therefore, a first task was required to obtain the combustion heat release profile for each engine running condition. The experimental inlet cylinder pressure is required to adjust the combustion profile on the model. In addition, it is necessary to know the timing of the injection and the fuel mass injected [29].

The materials of the each component of the engine and the heat transfer coefficients must be close to real conditions. It is necessary to adjust the pressure and the temperature in the exhaust. The geometry of the manifolds, exhaust line, intake line and EGR line must be performed according to reality: lengths, diameters, materials and heat exchangers. A multiplier for the heat transfer coefficient inside the cylinder, the inertia of the turbocharged and the compressor and turbine efficiencies are useful to calibrate methodically the model [30].

4. Model assessment

This section details the comparison between modeled and measured CO_2 concentration with the fast tracking device. Even though this device is able to sample with higher frequency than the traditional gas analyzer, its time resolution provides an approximate value of 8 ms, which is still far from crank-angle resolution. Depending on the system settings and, mainly, engine speed, around ten points can be sampled in one engine cycle (720 CAD). For this reason, the fast gas analyzer is measuring for several engine cycles (up to 200 consecutive cycles) and, under the assumption that the engine is running in steady condition, these measurements will fill the whole 720 CAD domain, as the following figures show.

Fig. 3 presents the results for the 2500 rpm and 19 bar BMEP running conditions, where the engine is operating with 4% EGR. Six plots are shown, corresponding to the measurements in the six locations described in Fig. 2. The CO_2 concentration is plotted against the crank-angle degree. As stated before not all the measured points correspond to the same engine cycle. All the points are plotted in red with certain level of transparency. The red solid line correspond to the average of all data, together with a light red band of two standard deviations wide (one above and one below the average values). The solid blue line corresponds to the predicted results provided by the 1D model. Together with the x-axis, labels indicating the period of the intake strokes for the four cylinders are added, following the firing order of the engine (1-3-4-2).

From the experimental point of view, some relevant information is obtained from the results. The variation of the CO_2 concentration along the engine cycle is reduced in locations #5 and #6, which are placed in the pipes of cylinder 4, since the air and EGR motion in that area should not be remarkable. Only when the intake valves of that cylinder open, a slight variation in the signals is observed. Locations #3 and #4 present slightly higher variations since they are placed in the pipes of cylinder 3, and the flow motion in the intake manifold in front of the central cylinders should become relevant. Location #1, which is placed in the intake manifold and not in the pipes, also reveals some variations in the CO_2 concentration but not so significant because the probe is close to one lateral end of the manifold. On the other side, location #2 is where the CO_2 concentration shows the largest variations since the probe in this location is in the central zone of the manifold and flow stream lines probably go through this area when either cylinder 1 or 2 perform the intake process.

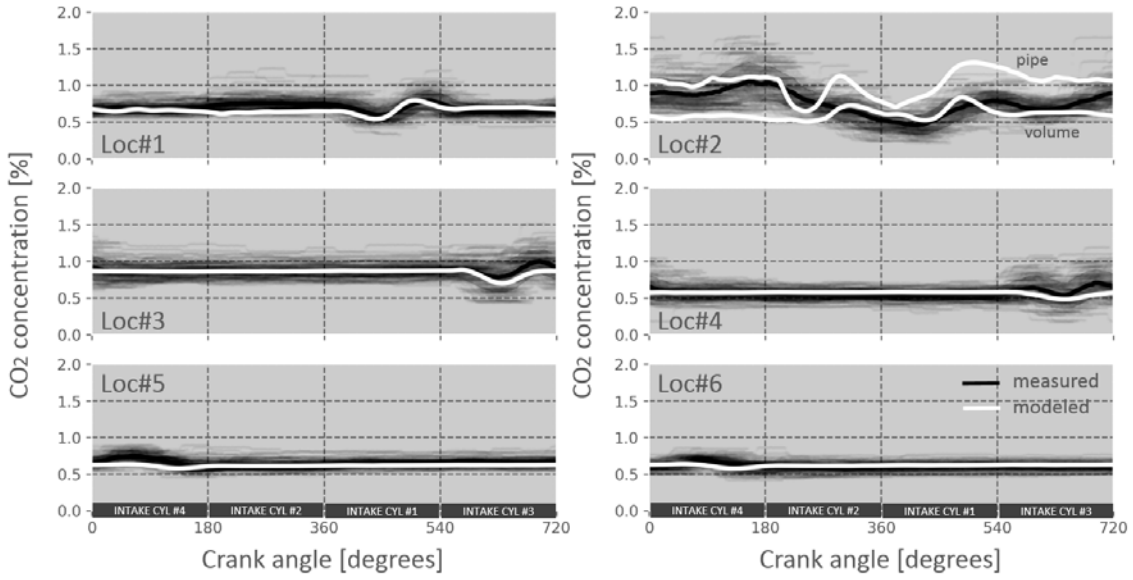

Figure 3. Instantaneous CO_2 concentration in several location of the intake manifold at 2500 rpm and 19 bar BMEP with 4% of EGR rate.

Regarding the comparison between experiments and the model prediction, it should be noted that the 1D model is able to reproduce with a good level of agreement the CO_2 concentration evolution in all the tested locations except location #2. The plot in location #2 includes the modeling results in two places of the intake manifold. Both plots correspond to the closest pipe and closest volume to the measurement probe. Since the

fluid dynamics inside the intake manifold follow a highly 3D pattern, a 1D engine model is not able to capture the concentration evolution in the same way that it is observed for other locations, which are placed in the pipes or in the lateral end of the manifold. However, it is observed that the experimental data falls between the chosen model places.

For the sake of brevity, not all the tested conditions introduced in Table 3 are plotted. If Fig. 3 constituted an example of engine full load conditions, Figs. 4, 5 and 6 represent partial load (2500 rpm and 10 bar BMEP with 17% of EGR), low load (1500 rpm and 3 bar BMEP with 3% of EGR) and very low load conditions (1500 rpm and 1 bar BMEP with 42% of EGR), respectively. The two last examples are both low load engine conditions but they have been chosen because they operate with very different EGR rates so they model performance in extreme situations can be assessed.

Focusing on Fig. 4, similar messages to those observed in Fig. 3 may apply. Firstly, location #2 presents again the largest CO_2 variations during the engine cycle, although, in this case, with 17% of EGR rate, the fluctuations in the intake manifold are lower (in relative terms) than those observed in Fig. 3, with 4% of EGR rate. And secondly, the 1D engine model is able to capture the signal evolutions, except for location #2.

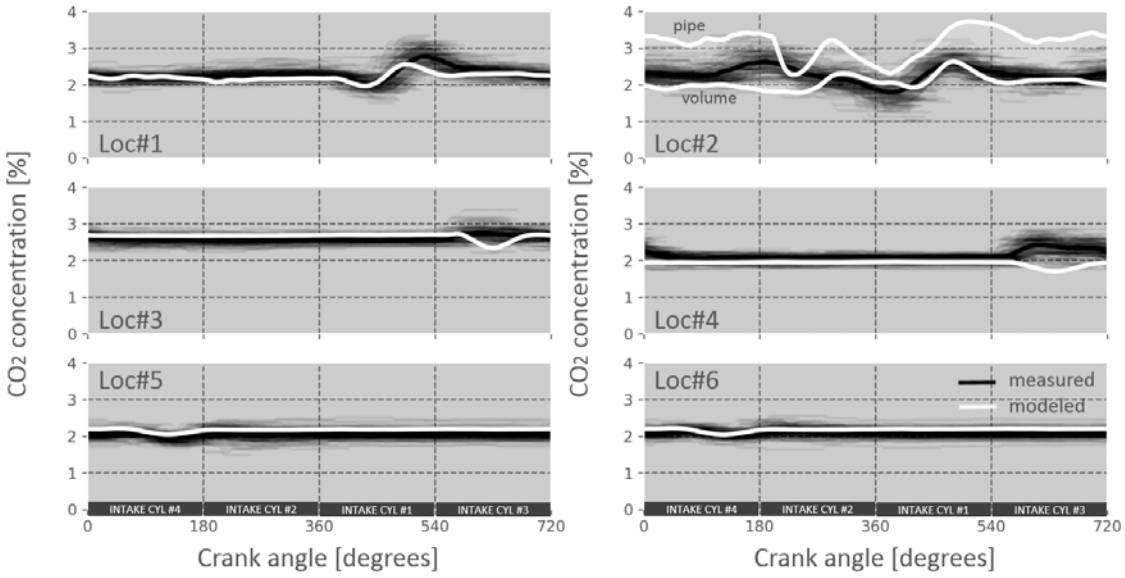

Figure 4. Instantaneous CO_2 concentration in several location of the intake manifold at 2500 rpm and 10 bar BMEP with 17% of EGR rate.

Fig. 5 presents the results for low load operation (1500 rpm and 3 bar BMEP) with a very reduced EGR rate (3%). This EGR rate is not the one typically found in real engines but was tested to confront the modeling results. On the other side, a low load and high EGR rate (42%) is found in Fig. 6, where the engine is running at 1500 rpm and 1 bar BMEP. Similar conclusions as the described before are derived from the plots.

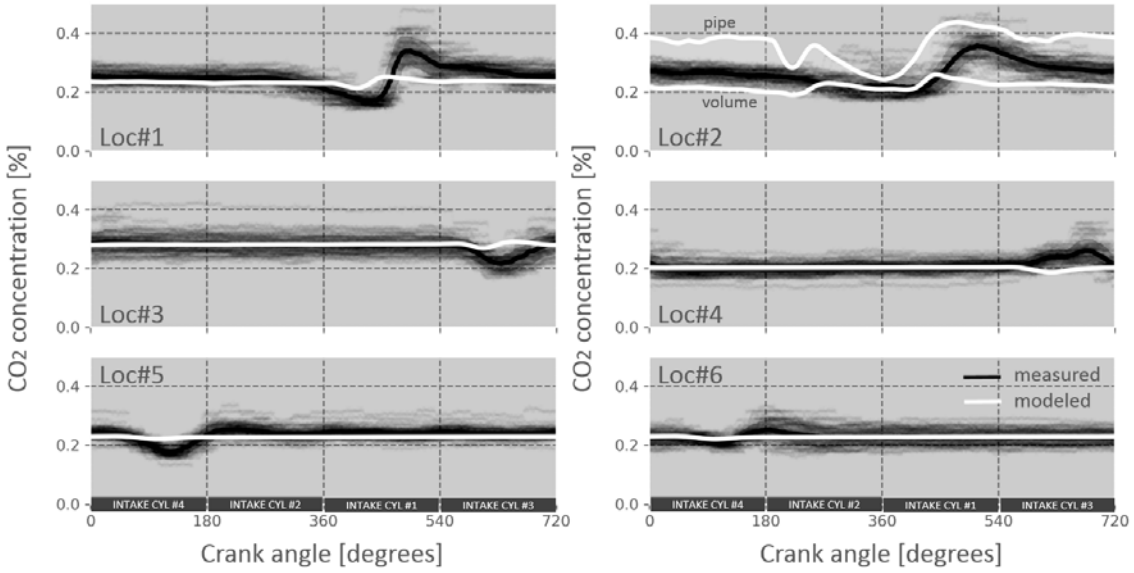

Figure 5. Instantaneous CO_2 concentration in several location of the intake manifold at 1500 rpm and 3 bar BMEP with 3% of EGR rate.

One additional comment would arise when observing the CO_2 traces in front of cylinder 3, i.e., locations #3 and #4. During the intake process in cylinder 3, the CO_2 concentration behaves oddly: sometimes a drop occurs, sometimes there is an increase, and sometimes there is an increase after an initial drop. This behavior does not happen equally in both pipes of cylinder 3, as can be observed in Figs. 5 and 6, where location #3 starts with a reduction in the CO_2 concentration while location #4 initiates with a slight increase. The local fluid dynamics phenomena may be the root cause for this behavior and the 1D model is not always capable to capture. For instance, the evolutions in low load engine conditions with high EGR rate shown in Fig. 6 present the opposite behavior: measured CO_2 concentration in location #3 presents a sudden reduction while the model predicts an increase; however, location #4 reveals the opposite performance. It is important to keep this in mind because the predictive model capability for the cylinders EGR dispersion will be determined by the ability to reproduce the CO_2 concentration in the pipes during the intake stroke; a perfect match between model and experimental data while the intake valves are closed does not necessarily mean a good EGR dispersion prediction.

Another important remark that derives from the observation of empirical data is that there is always a presence of CO_2 in the pipes, even in the situations when the engine is running with very low EGR rates (3% and 4%), as in Figs. 3 and 5. The concentration in the pipes of the lateral cylinders provides nearly constant values while the central cylinders present higher fluctuations, with ranges that move from 50% over the average value, when the engine is running with high EGR rates, to 100% when the EGR rate is reduced.

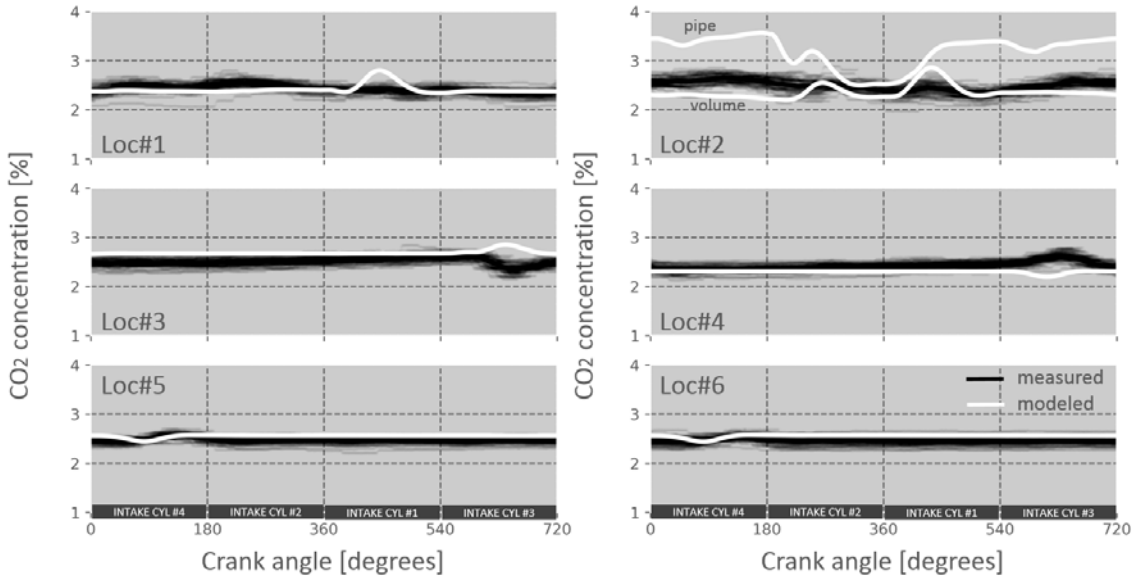

Figure 6. Instantaneous CO_2 concentration in several location of the intake manifold at 1500 rpm and 1 bar BMEP with 42% of EGR rate.

5. EGR dispersion results

Once the 1D engine model is evaluated with instantaneous CO_2 concentration inside the intake manifold during an engine cycle, the EGR dispersion among the cylinders is the topic presented in this section. The results discussed here correspond to a direct comparison between experimental EGR calculation in each pipe obtained with Eq. (1) using measurements acquired with the time-averaged gases analyzer and the predicted results from the 1D model.

Several engine running conditions are evaluated to cover a wide range of engine operation in terms of engine speed and load. The performance of the model is demonstrated with several levels of EGR dispersion, which are achieved by proper modification of the regulation valves in the three EGR branches described in Section 2. Even off-design levels of EGR dispersion were tested to check the model predictive capabilities under extreme situations. In specific operating conditions, a variation of the EGR rate and its influence on the EGR dispersion is also assessed.

5.1. Metrics definition

There are eight outputs from the model to be compared with experimental data: the EGR rate in each intake pipe. Direct visualization of these data in bar plots comparing predicted and measured results is possible but not practical for the 29 engine conditions. Therefore, the definition of some metrics is helpful to analyze the EGR dispersion in a comprehensive manner. The non-dimensional root mean squared error summarizes all the differences between model and experiments in a scalar. It results from the simple addition of the differences in all the cylinders to the square (in order to avoid that negative errors would decrease the global error) and divided by the average of the experimental EGR rate. The expression is given in Eq. (9):

$$ndRMSE = \frac{\sqrt{\sum_{i=1}^{n}(x_{i,mod}-x_{i,exp})^2/n}}{\bar{x}_{exp}} \quad (9)$$

Where *n* is the number of cylinders, *i* denotes the cylinder, subscripts *mod* and *exp* indicate model and experiment, respectively, and $\bar{x}$ is the average of all the cylinders. Since the EGR dispersion analysis should be evaluated in the cylinders, where the combustion process takes place, the comparison between experiments and model is performed from a cylinder point of view and not from an intake pipe perspective. The calculation of the EGR rate in the cylinders is carried out by averaging the values from the two corresponding intake pipes. The ndRMSE is a non-dimensional value but in the following analysis it is expressed in percentage format.

Together with the non-dimensional RMSE, simple comparisons can be made from a cylinder perspective, which will lead to an additional metric: the difference between the model and the experiment from all the pipes for a given running condition. This metric can be calculated: (a) in absolute terms, whose unit will be percentage points of EGR level (absolute error), and (b) in relative terms, dividing the difference between the experimental and modeling values by the experimental value, whose unit will be percentage (relative error).

The non-dimensional root mean squared error (ndRMSE), absolute error (AE) and relative error (RE) compare predicted and measured results, while the following metrics can be applied to either the model or the experimental data and do not provide any information about the performance of the model. The standard deviation can be computed to evaluate the differences in the pipes related to the average value. So this is a metric to evaluate the EGR dispersion, whose expression is given in Eq. (10):

$$\sigma = \sqrt{\sum_{i=1}^{n}(x_i - \bar{x})^2/n} \quad (10)$$

If a normalized value with the EGR rate that the engine is running is desired, then the coefficient of variance provided in Eq. (11) is needed:

$$COV = \frac{\sqrt{\sum_{i=1}^{n}(x_i-\bar{x})^2/n}}{\bar{x}} \quad (11)$$

A symmetry factor SF [31] can be defined taking into account that every pipe from 1 to 4 will have a geometrical opposed pipe, from pipe 8 to 5. Hence, this factor is defined as:

$$SF = \sum_{i=1}^{4}\frac{(x_i-x_{9-i})^2}{\bar{x}^2} \quad (11)$$

Where the subscript refers to the number of the intake pipe. Again, the differences are computed to the square to avoid the cancellation between positive and negative differences. The symmetry factor is always a positive value and it provides values close to zero when the spatial profile of the EGR dispersion is symmetric. The higher the SF value, the more asymmetric spatial pattern is found.

Finally, another metric to evaluate the shape of the spatial distribution of the results in the pipes (either predicted or measured) is the convexity factor (CF) [31] given by Eq. (12):

$$CF = \sum_{i=2}^{7} \left(x_i - \frac{(x_{i+1} + x_{i-1})}{2} \right) \cdot \frac{1}{\bar{x}} \quad (12)$$

Where, again, the subscript relates to the intake pipe. While the other metrics provided scalars greater than zero, the CF can be a positive or a negative number. An inspection of the previous expression would lead to conclude that flat spatial EGR distributions in the pipes provide convexity factors close to zero, while positive values indicate a convex distribution (i.e. higher values in the pipes located in the extremes) and negative values mean concave profiles (i.e. higher values in the central pipes).

5.2. *Results with controlled EGR dispersion*

Figure 7 shows the measured and predicted EGR rate in the intake pipes with the engine running at 2000 rpm and 6 bar BMEP. The engine runs with an average EGR rate around 24% and the three valves that regulate the EGR dispersion are open in specific positions to obtain a very low EGR dispersion in the cylinders. The numbers above the bars correspond to the EGR rate in each pipe, so a simple difference between measured and predicted data provides the absolute error in each pipe. The numbers inside the bars corresponding to the predicted results from the model are the relative errors between predicted and measured values in each pipe. A legend with the non-dimensional RMSE and the experimental information concerning the average EGR rate, the symmetry factor and the convexity factor is also displayed in the plot.

The spatial pattern of the EGR in the pipes is nearly flat so the symmetry and convexity factors calculated from the experimental information are close to zero. The 1D engine model predictions are reasonably accurate in this case. The large differences in the pipes of cylinder 2 are cancelled when the average EGR in the cylinder is calculated, since the predicted results in one pipe are overestimated while an under-prediction appears in the other pipe. Something similar occurs in cylinder 3. As a global comparison of all the cylinders, the non-dimensional RMSE, which accounts for the deviations from experimental and modeling results, is lower than 5%.

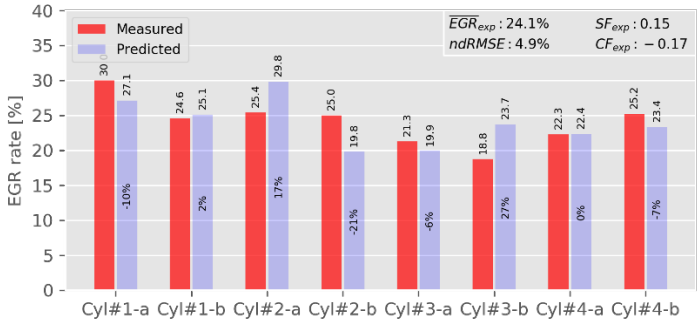

Figure 7. Measured and predicted EGR rate in the pipes at 2000 rpm and 6 bar BMEP with 24% EGR rate and symmetric position for the EGR dispersion valves.

The engine running conditions are kept constant in terms of engine speed, torque and average EGR rate but the EGR dispersion regulation valves are operated to have an

asymmetric spatial distribution. This situation is depicted in Fig. 8, where two arbitrary positions for the EGR valves provide more EGR to cylinders 3 and 4 (left plot) or to cylinders 1 and 2 (right plot). As a consequence, both the symmetric and convexity factors increase. The 1D engine model, calibrated with the corresponding effective area in the EGR regulation valves, is not performing with the same accuracy level as in Fig. 7. The model overestimates the EGR in the intake manifold side where the EGR introduction was promoted. Predicted values in pipes in cylinder 4 in the left plot (or cylinder 1 in the right plot) are remarkable higher than in the measurements. Therefore, the non-dimensional RMSE increases up to approximately 30% in both cases.

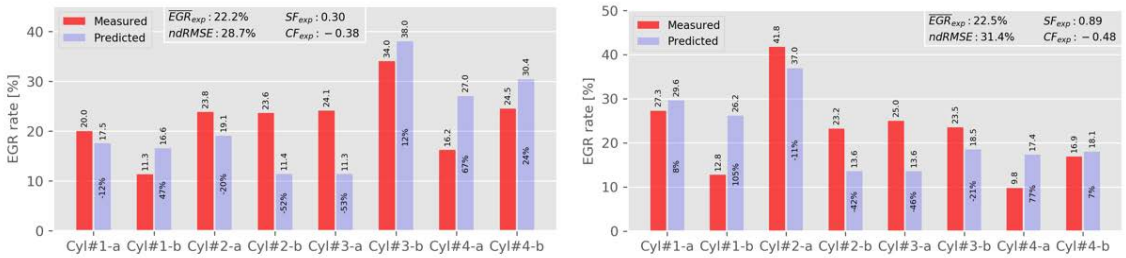

Figure 8. Measured and predicted EGR rate in the pipes at 2000 rpm and 6 bar BMEP with 22% EGR rate and two arbitrary asymmetric positions for the EGR dispersion valves.

The engine running conditions are now changed to 3000 rpm and 20 bar BMEP with around 12% of EGR rate. This engine condition at full load did not activate the EGR strategy in engine a few years ago. Figure 9 shows two situations: on the left, the EGR valves position are calibrated to achieve a very low dispersion level while, on the right, an arbitrary position for the EGR valves provide more EGR to cylinders 3 and 4. Hence, the symmetric factor is close to zero on the left plot while it increases up to 3 in the high dispersion level situation on the right. The convexity factor is low in both cases. The 1D engine model performs with a good agreement to the experimental results in both conditions as observed in the low values of the non-dimensional RMSE, with values lower than 2% and 6%, respectively.

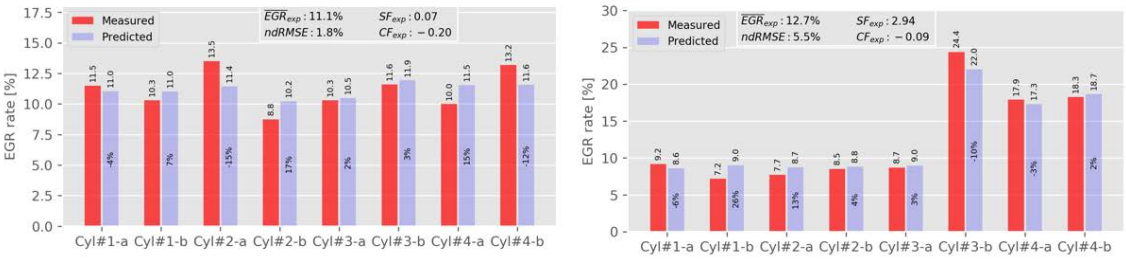

Figure 9. Measured and predicted EGR rate in the pipes at 3000 rpm and 20 bar BMEP with around 12% EGR rate, with symmetric (left) and asymmetric (right) positions for the EGR dispersion valves.

5.3. *Results with EGR rate variations*

Figure 10 presents the comparison at 1500 rpm and 1 bar BMEP with different EGR rates: 42% (top, left), 29% (top, right), 22% (bottom, left) and 7% (bottom, right). The EGR regulation valves were set to provide a low EGR dispersion with 42% EGR and

remained in those positions in the rest of the EGR rates. From the experiments, symmetry and convexity factors are close to zero in all the conditions, but the one with the lowest EGR rate, where more EGR is detected in the central pipes. In fact, the convexity factor increases from nearly zero to 0.23 in this case. The model performs with non-dimensional RMSE values lower than 8% in the three cases with high EGR rates. With the lowest EGR rate, although the engine model reveals higher EGR levels in the central pipes than in the rest, the phenomenon is not captured as measured in the experiment and the error increases up to 18.5%.

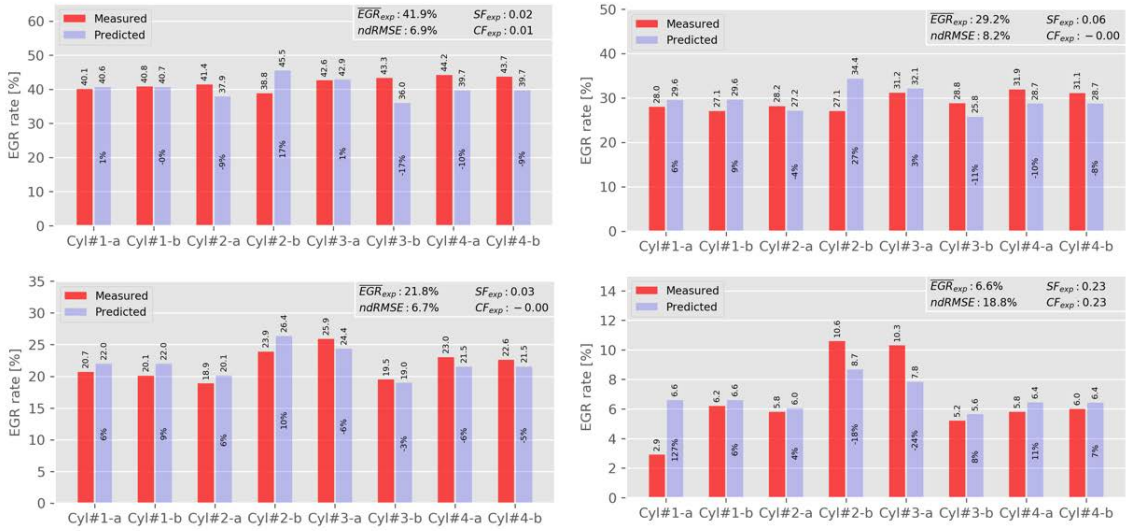

Figure 10. Measured and predicted EGR rate in the pipes at 1500 rpm and 1 bar BMEP with 42% (top, left), 29% (top, right), 22% (bottom, left) and 7% (bottom, right) EGR rates and symmetric positions for the EGR dispersion valves.

The COV is plotted against the averaged EGR rate in Fig.11. The results from the engine tests are shown in red circles, while the model data is given with blue crosses. Together with these dots, linear trends are included. An increase in the COV, which is a metric for the EGR dispersion, is observed as the EGR rate reduces. This behavior is clearly detected in the engine tests. However, the model is not able to capture this phenomenon, mainly for EGR rates lower than 10%.

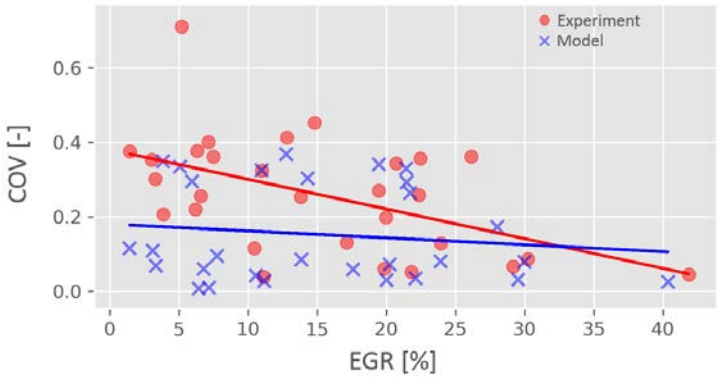

Figure 11. Measured and predicted COV as a function of the EGR rate in the 29 engine running conditions.

5.4. *1D engine model performance*

The absolute and relative errors in the cylinders for the 29 engine running conditions are depicted in Fig. 12. Each dot represents a comparison in a cylinder. Red dots refer to the cylinders at the end of the engine block (either cylinder 1 or 4), while blue dots correspond to the cylinders in the central part (either cylinder 2 or 3). A positive value means that the model is overestimating the EGR rate in a given cylinder. In general terms, the 1D engine model over-predicts the experimental results concerning the cylinders 1 and 4; the opposite occurs for the other cylinders. The representation of the real intake manifold with 1D and 0D elements allows to have some flow motion from the central part of the manifold to its ends but when cylinders 2 and 3 are in the intake stroke, the flow motion from the pipes of cylinders 1 and 4 is less likely to happen than from the intake line. Therefore, the path for fluid motion between cylinders 1 and 4 to cylinders 2 and 3 is easier in the real 3D geometry rather than in the 0D-1D simple approach. Maximum absolute errors of 10% in EGR rate take place when the engine operates with EGR rates around 20%. On the other hand, maximum relative errors up to 80% occur at reduced EGR rates (i.e. lower than 10%).

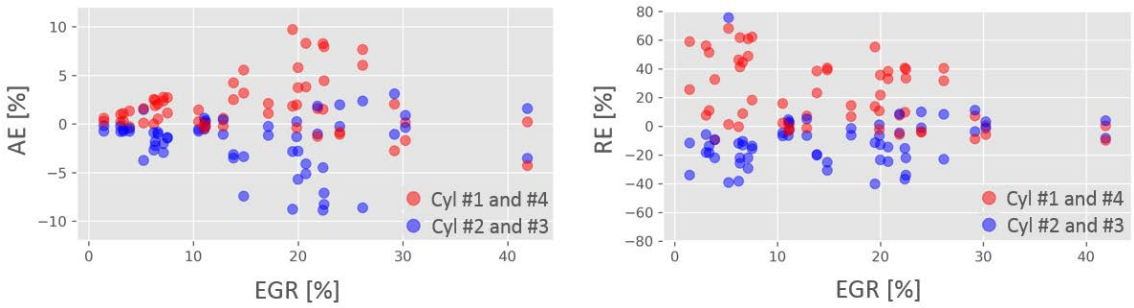

Figure 12. Cylinder EGR absolute (left) and relative (right) errors as a function of the EGR rate in the 29 engine running conditions (red dots: cylinders 1 and 4; blue dots: cylinders 2 and 3).

Figure 13 correlates the relative errors results with the non-dimensional RMSE. There is an obvious relation between both metrics. Large differences in the model predictions show high values for both the RE and ndRMSE. If the ndRMSE is lower than 10%, the maximum relative errors do not exceed 20%. The same color code for the cylinders is applied in Fig. 13 than in Fig. 12. While for ndRMSE values higher than 10%, the model presents a clearly overestimation in the results for cylinders 1 and 4, this is not so evident for ndRMSE values lower than 10%.

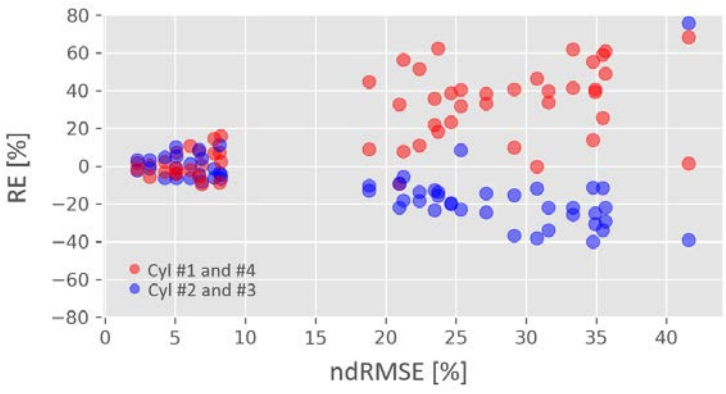

Figure 13. Cylinder EGR relative errors as a function of the non-dimensional RMSE in the 29 engine running conditions (red dots: cylinders 1 and 4; blue dots: cylinders 2 and 3).

A simple inspection of the data presented in Fig. 12 and 13, with a cloud of dots ranging from -40% to 80% in relative errors, does not allow to give answers to: (a) the percentage of engine simulations that obtain a specific threshold of relative error, and (b) which engine running conditions the model is able to predict with a good level of agreement. Therefore, a thorough analysis of the results is needed. The left plot in Fig. 14 shows in the Y-axis the percentage of simulations that achieve a maximum relative error (MRE) found in the X-axis. There are two curves inside: the red one corresponds to the analysis when all the simulations are considered, while the blue one shows the information without considering the engine running conditions with an EGR rate lower than 10%. The plot on the right is similar but replacing the X-axis with the non-dimensional RMSE.

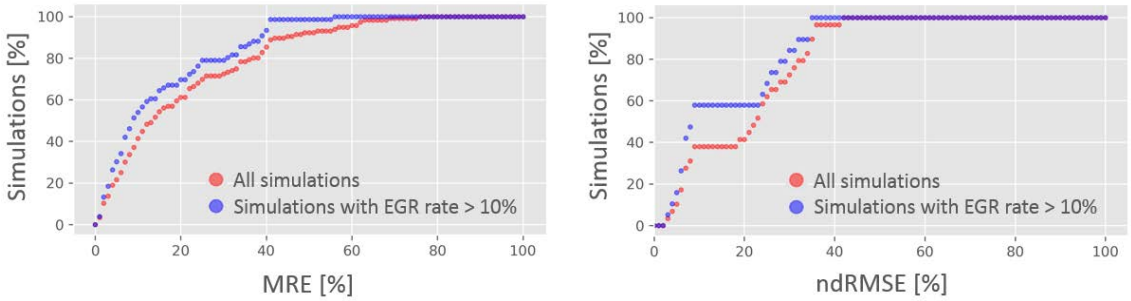

Figure 14. Simulations percentage with lower values of maximum RE (left) and non-dimensional RMSE (right) with all engine conditions (in red) and engine operation with EGR rate higher than 10% (in blue).

From the data in Fig. 14, the 60% of all the simulations provide maximum relative errors lower than 20%. If the engine operations with EGR rate lower than 10% are filtered out, the percentage of simulations increases. For instance, up to 80% of the simulations provide results with relative errors lower than 25% and nearly all the simulations run with relative errors lower than 40%. Concerning the non-dimensional RMSE, 40% of all the simulations provide an error lower than 10%, while the percentage of simulations increases up to 60% if the engine runs with EGR rates higher than 10%.

The last question would be to find out why the model performs so different in terms of cylinder EGR accuracy and, in particular, which engine running conditions have to be met to rely on the data predicted by the 1D. The experimental data for symmetry and convexity factors are plotted against the non-dimensional RMSE in Fig. 15. It is important to remind that SF takes only positive values, being zero a perfect symmetric spatial EGR dispersion, while CF takes positive and negative values, being zero a completely flat distribution; for visualization purposes, the two Y-axes share the zero value. Engine tests with high convexity factors (in absolute value) and extremely high symmetry factors provide bad model prediction values concerning the non-dimensional RMSE. There are simulations that show high errors with reduced CF and SF but these simulations correspond to low EGR rate engine conditions.

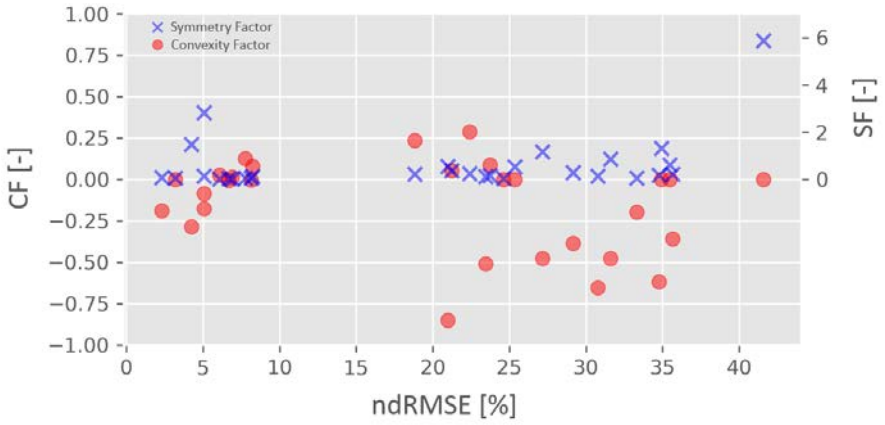

Figure 15. Symmetry and convexity factors from the experiments as a function of the non-dimensional RMSE in the 29 engine running conditions.

6. Conclusions

The performance of a 1D modeling approach to predict the high pressure EGR transport and dispersion in the cylinders of an automotive engine was evaluated in this study. An exhaustive experimental campaign was fulfilled including EGR operation in full load conditions. Up to 29 engine running conditions covering the engine map together with variations in the EGR rate in specific engine speed and engine torque set points were tested. A fast CO_2 tracking device was used to assess the 1D model results in 6 locations of the intake manifold. Since the sampling frequency of this equipment provides around 10 measurements per engine cycle, several consecutive engine cycles were acquired in order to have a pseudo-evolution of the CO_2 with crank-angle resolution. From the experimental domain, a specific hardware was setup to promote and control different levels of EGR dispersion in the cylinders.

A 1D engine model was employed to simulate the experiments in the test bench. Instantaneous CO_2 concentration predictions in the 6 locations inside the intake manifold lead to the following: (a) predictions in locations in the center of the manifold (location #2) are difficult to be captured by the model due to the highly 3D behavior of the flow and the compactness of current intake manifolds; and (b) predictions in the pipes offer better correlations. However, the instantaneous evolutions during the intake stroke of the corresponding cylinder are not always properly captured.

Comparisons in EGR averaged values in the pipes were also discussed to assess the performance of the 1D model. Globally, the model underestimates the EGR rates in the central cylinders (2 and 3), while an overestimation occurs in the cylinders at the engine block ends (1 and 4). From the experimental perspective, the normalized EGR standard deviation increases with low EGR rates. This phenomenon is not captured by the model, which shows maximum relative errors in some cylinders around 60%. The prediction in terms of in-cylinder EGR improves to differences lower than 40% if the engine operating points with an average EGR rate lower than 10% are excluded. In this situation, 80% of the predicted in-cylinder EGR rates have differences lower than 25% when compared to experiments. The prediction performance of the 1D model is not remarkable in all simulations. There is an obvious correlation between the individual errors in the cylinders and the global metric to evaluate the prediction performance, which is the root mean

squared error. The RMSE present values up to 40%. However, 40% of the simulations provide RMSE lower than 10%, linked to relative errors in the cylinders lower than 20%. The simulations with RMSE higher than 10% reproduce experimental profiles for the EGR spatial distribution with remarkable values of the convexity factor or symmetry factor. Therefore, the model provides best results when reproducing engine situations with high EGR rates and an HP-EGR system that enables a moderate EGR dispersion, being both conditions typically found in current automotive engines.

7. References

1. Ming Zheng, Graham T. Reader, J. Gary Hawley. “Diesel engine exhaust gas recirculation – a review on advanced and novel concepts”, Energy Conversion and Management 45 (2004) 883-900.

2. Deepak Agarwal, Shrawan Kumar Singh, Avinash Kumar Agarwal. “Effect of Exhaust Gas Recirculation (EGR) on performance, emissions, deposits, and durability of a constant speed compression ignition engine”, Applied Energy 88 (2011) 2900-2907.

3. Ladommatos N, Abdelhalim SM, Zhao H, Hu Z. “The dilution, chemical, and thermal effects of exhaust gas recirculation on diesel engine emissions – Part 1: Effect of reducing inlet charge oxygen”, SAE Technical Paper 961165, 1996.

4. Ladommatos N, Abdelhalim SM, Zhao H, Hu Z. “The dilution, chemical, and thermal effects of exhaust gas recirculation on diesel engine emissions – Part 2: Effects of carbon dioxide”, SAE Technical Paper 961167, 1996.

5. Ladommatos N, Abdelhalim SM, Zhao H, Hu Z. “The dilution, chemical, and thermal effects on exhaust gas recirculation on diesel engine emissions – Part 3: Effects of water vapor”, SAE Technical Paper 971659, 1997.

6. Ladommatos N, Abdelhalim SM, Zhao H, Hu Z. “The dilution, chemical, and thermal effects of exhaust gas recirculation on diesel engine emissions – Part 4: Effects of carbon dioxide and water vapor”, SAE Technical Paper 971660, 1997.

7. José Manuel Luján, Vicente Dolz, Javier Monsalve-Serrano, Juan Antonio López-Cascant. “New anti-pollution regulation for Euro 6 diesel vehicles”, Técnica Industrial 318 (2017) 28-33. DOI:10.23800/9939.

8. José Manuel Luján, Héctor Climent, Santiago Ruiz and Ausias Moratal, “Influence of ambient temperature on diesel engine raw pollutants and fuel consumption in different driving cycles”, International Journal of Engine Research 20 (8-9) (2019) 877-888. DOI: 10.1177/1468087418792353.

9. José Galindo, Hector Climent, Olivier Varnier and Chaitanya Patil, “Effect of boosting system architecture and thermomechanical limits on diesel engine performance: Part II—transient operation”, International Journal of Engine Research 19 (8) (2018) 873-885. DOI: 10.1177/1468087417732264.

10. J.R. Serrano, P. Piqueras, R. Navarro, D. Tarí, C.M. Meano, “Development and verification of an in-flow water condensation model for 3D-CFD simulations of humid air streams mixing”, Computers and Fluids 167 (2018) 158-165.

11. J.Galindo, P.Piqueras, R.Navarro, D.Tarí, C.M.Meano, “Validation and sensitivity analysis of an in-flow water condensation modelfor 3D-CFD simulations of humid air streams mixing”, International Journal of Thermal Sciences 136 (2019) 410-419. https://doi.org/10.1016/j.ijthermalsci.2018.10.043.

12. José Manuel Luján, Héctor Climent, Francisco José Arnau, Julián Miguel-García, “Analysis of low-pressure exhaust gases recirculation transport and control in transient operation of automotive diesel engines” Applied Thermal Engineering 137 (2018) 184-192. https://doi.org/10.1016/j.applthermaleng.2018.03.085

13. Vicente Macián, José Manuel Luján, Héctor Climent, Julián Miguel-García, Stéphane Guilain and Romain Boubennec, “Cylinder-to-cylinder high-pressure exhaust gas recirculation dispersion effect on opacity and NOx emissions in a diesel automotive engine” International Journal of Engine Research (2020). https://doi.org/10.1177/1468087419895401

14. Mirko Baratta and Ezio Spessa, “Numerical Simulation Techniques for the Prediction of the Fluid-Dynamics, Combustion and Performance in IC Engines Fuelled by CNG.” Computational Simulations and Applications, chapter 12 (2011) 259-286. DOI: 10.5772/25081.

15. Aleksandrs Korsunovs, Felician Campean, Gaurav Pant, Oscar Garcia-Afonso and Efe Tunc, “Evaluation of zero-dimensional stochastic reactor modelling for a Diesel engine application.” International Journal of Engine Research 21 (4) (2020) 592-609. DOI: https://doi.org/10.1177/1468087419845823.

16. Adèle Poubeau, Arthur Vauvy, Florence Duffour, Jean-Marc Zaccardi, Gaetano de Paola and Marek Abramczuk, “Modeling investigation of thermal insulation approaches for low heat rejection Diesel engines using a conjugate heat transfer model.” International Journal of Engine Research 20 (1) (2019) 92-104. DOI: https://doi.org/10.1177/1468087418818264

17. Peter Andruskiewicz, Paul Najt, Russell Durrett, Scott Biesboer, Tobias Schaedler and Raul Payri, “Analysis of the effects of wall temperature swing on reciprocating internal combustion engine processes.” International Journal of Engine Research 19 (4) (2018) 461-473. DOI: https://doi.org/10.1177/1468087417717903

18. Peter Andruskiewicz, Paul Najt, Russell Durrett and Raul Payri, “Assessing the capability of conventional in-cylinder insulation materials in achieving temperature swing engine performance benefits.” International Journal of Engine Research 19 (6) (2018) 599-612. DOI: https://doi.org/10.1177/1468087417729254

19. José Galindo, Roberto Navarro, Luis Miguel García-Cuevas, Daniel Tarí, Hadi Tartoussi and Stephane Guilain. “A zonal approach for estimating pressure ratio at compressor extreme off-design conditions.” International Journal of Engine Research 20 (4) (2019) 393-404. DOI: 10.1177/1468087418754899.

20. Julien Bohbot, Christos Chryssakis and Marjorie Miche, “Simulation of 4-Cylinder Turbocharged Gasoline Direct Injection Engine Using a Direct Temporal Coupling Between a 1D Simulation Software and a 3D Combustion Code”, SAE Technical Paper 2006-10-16, 2006, SAE International DOI: 10.4271/2006-01-3263

21. Federico Millo, Paolo Ferrero Giacominetto, Marco Gianoglio Bernardi, “Analysis of different exhaust gas recirculation architetures for passenger car Diesel engines”. Applied Energy 98 (2012) 79-91.

22. Robert M. Siewert, Roger B. Krieger, Mark S. Huebler, Prafulla C. Baruah, Bahram Khalighi and Markus Wesslau, “Modifying and Intake Manifold to Improve Cylinder-to-Cylinder EGR Distribution in a DI Diesel Engine Using Combined CFD and Engine Experiments”, SAE Technical Paper 2001-01-3685, 2001, http://dx.doi.org/10.4271/2001-01-3685.

23. Hardik Lakhlani, Jyotirmoy Barman, Karan Rajput and Angshuman Goswami, “Experimental Study of EGR Mixture Design and its Influence on EGR Distribution Across the Cylinder for NOx-PM Tradeoff”, SAE Technical Paper 2013-11-27, 2013 SAE Int. doi: 10.4271/2013-01-2743.

24. Pavlos Dimitriou, Richard Burke, Colin Copeland, Sam Akehurst, “Study on the Effects of EGR Supply Configuration on Cylinder-to-Cylinder Dispersion and Engine Performance Using 1D-3D Co-Simulation”, SAE Technical Paper 2015-11-17, 2015.

25. J.M. Luján, H. Climent, L.M. García Cuevas, A. Moratal, “Volumetric efficiency modelling of internal combustion engines based on a novel adaptative learnig algorithm of artificial neural networks” Applied Thermal Engineering 123 (2017) 625-634.

26. Galindo, J., Serrano, J. R., Arnau, F. J., and Piqueras, P., "Description of a Semi-Independent Time Discretization Methodology for a One-Dimensional Gas Dynamics Model." ASME. *J. Eng. Gas Turbines Power*. May 2009; 131(3): 034504. https://doi.org/10.1115/1.2983015

27. D.E. Winterbone and R. J. Pearson, Theory of engine manifold design: wave action methods for IC engines. Wiley-Blackwell (2000).

28. J.R. Serrano, H. Climent, P. Piqueras, O. García-Alfonso, “Analysis of shock capturing methods for chemical species transport in unsteady compressible flow.” Mathematical and Computer Modelling 57 (7-8) (2013) 1751-1759.

29. L. Kaprielian, “Modélisation 0D pour la combustion dans les moteurs à allumage commandé : développements en proche paroi et dans le front de flamme.” PhD Thesis, Arts et Métiers Paris Tech, 2015.

30. D. Chalet, M. Lesage, M. Cormerais, T. Marimbordes – “Nodal modelling for advanced thermal-management of internal combustion engine.” Applied Energy, Volume 190, pp. 99-113, ISSN 0306-2619, DOI 10.1016/j.apenergy.2016.12.104, 2017

31. José Galindo, Héctor Climent, Roberto Navarro, Guillermo García-Olivas, Stéphane Guilain, Romain Boubennec, “Effect of Numerical Configuration on Predicted EGR Cylinder-to-Cylinder Dispersion,” SAE Technical Paper 2020-01-1113, 2020, doi:10.4271/2020-01-1113.